Journal of Power Sources 192 (2009) 556–561

Contents lists available at ScienceDirect

Journal of Power Sources

journal homepage: www.elsevier.com/locate/jpowsour

An onboard hydrogen generation method based on hydrides and water recovery for micro-fuel cells

L. Zhu [a,*], V. Swaminathan [a], B. Gurau [b], R.I. Masel [b], M.A. Shannon [a]

[a] Department of Mechanical Science and Engineering, University of Illinois at Urbana Champaign, 1206 W. Green Street, Urbana, IL 61801, USA
[b] Department of Chemical and Biomolecular Engineering, University of Illinois, 600 South Mathews Avenue, Urbana, IL 61801, USA

ARTICLE INFO

Article history:
Received 27 February 2009
Received in revised form 19 March 2009
Accepted 19 March 2009
Available online 27 March 2009

Keywords:
Micro-fuel cell
Water recovery
Hydride
Onboard hydrogen generation

ABSTRACT

Micro-proton exchange membrane fuel cells are considered to be the next generation power sources for micro-scale power applications, but onboard hydrogen storage and generation with high energy density at the small scale is still a technical barrier. This paper introduces a hydrogen generation method based on an onboard hydride fuel and a byproduct water recovery mechanism for micro-hydrogen PEM fuel cells. The water recovery is carried out by water diffusion from the more humid cathode side to the less humid anode side through the proton exchange membrane. The micro-fuel cells based on this water recovery method were constructed and tested. The results demonstrate that the relative humidity has a significant affect on the fuel cell performance as well as the opening area on the cover layer, the type of hydrides, and the thickness of the Nafion membrane also can affect the fuel cell performance. A 10 mm^3 prototype water recovery micro-fuel cell has been built and tested, and the device has produced a maximum power density of 104 $W\,L^{-1}$ and a maximum energy density of 313 $W\,h\,L^{-1}$.

1. Introduction

Proton exchange membrane (PEM) hydrogen fuel cells have received considerable attention over the past decade as a promising alternative to the traditional power generation technologies due to their relatively high power densities, high energy densities, environmental friendly byproducts, and rapid recharging [1–7]. However, on-board hydrogen storage and generation with high energy density is still challenging for hydrogen fuel cells. According to the U.S. Department of Energy's Freedom Car Program targets, the gravimetric density of hydrogen should be at least 6 wt.%, and the volumetric density should be at least 45 $kg\,m^{-3}$ by 2010. The targets for 2015 are 9 wt.% for gravimetric density and 81 $kg\,m^{-3}$ for volumetric density [8].

Hydrogen storage and generation methods have been widely explored for decades including compressed hydrogen gas, liquid hydrogen, adsorption on carbon nanotubes [9–11] and metal organic frameworks (MOFs) [12], hydrogen reformation [13,14], and metal and chemical hydrides [15,16]. However, the low energy density, high pressure and low temperature requirements, plus relatively high costs, make many storage methods unpractical for micro-fuel cell applications. Among these methods, metal and chemical hydrides have shown the potential for micro-scale hydrogen storage and generation because of the high theoretical hydrogen volumetric density, which is the more critical target due to constraints on fuel storage space at small scales [17]. To this end, several metal and chemical hydrides have been studied to build onboard hydrogen generators for micro-fuel cells. For instance, a catalytic hydrolysis reaction of an alkaline sodium borohydride ($NaBH_4$) solution has been widely reported [18–27]. However, a diluted $NaBH_4$ solution will reduce the overall fuel energy density, which is not desired in micro-scale systems. In 2003, Kong et al. reported a reactor that utilized the hydrolysis reaction of hydrides and water vapor. A nickel mesh basket was used to contain hydride powders and liquid water was added to the bottom of the reaction vessel [28]. However, the volume of the nickel mesh basket is about 3% of the volume of the whole device, which decreased the energy density of the whole device. Recently, researchers have developed millimeter scale hydrogen generators integrated with micro-PEM fuel cells [29–31]. The hydrogen generation is based on the hydrolysis reaction of hydrides, calcium hydride (CaH_2) and lithium aluminum hydride ($LiAlH_4$), with water vapor. The hydride powders and liquid water were loaded into separated microchambers and water vapor delivery was controlled by a spiral microchannel [31], or passive microvalves [29,30]. These integrated micro-power generators have about 200 $W\,h\,L^{-1}$ energy density, but the liquid water has to be carried onboard, which consumes additional space and increases the overall volume and weight of the associated power generator.

* Corresponding author. Tel.: +1 217 244 7301; fax: +1 217 244 6534.
E-mail address: lzhu@illinois.edu (L. Zhu).

0378-7753/$ – see front matter © 2009 Elsevier B.V. All rights reserved.
doi:10.1016/j.jpowsour.2009.03.033

Table 1
Hydrogen fuel cell reaction and theoretical energy densities of some hydrides if water is not included as onboard fuel.

Hydrolysis reactions	Theoretical energy density ($W\,h\,L^{-1}$) (when the fuel cell operates at 0.6 V)
$LiBH_4 + 4H_2O \rightarrow H_3BO_3 + LiOH + 4H_2$	2202
$MgH_2 + 2H_2O \rightarrow Mg(OH)_2 + 2H_2$	2601
$LiH + H_2O \rightarrow LiOH + H_2$	1156
$LiAlH_4 + 4H_2O \rightarrow Al(OH)_3 + LiOH + 4H_2$	2516
$CaH_2 + 2H_2O \rightarrow Ca(OH)_2 + 2H_2$	1947
Hydrogen fuel cell reaction	
$2H_2 + O_2 \rightarrow 2H_2O$	

In order to further increase the energy density of the integrated micro-power generators, water should not be carried onboard, but recovered from the cathode reaction of the hydrogen fuel cell and the ambient moisture. The fuel cell reaction of a hydrogen PEM fuel cell and some hydrolysis reactions are shown in Table 1. As seen in the reaction formulas in Table 1, the numbers of moles of water and hydrogen are the same for all the reactions. If all of the byproduct water can be recycled to the hydride chamber to generate hydrogen, the micro-fuel cell can maintain its performance without additional water. This approach reduces the overall size and weight of the system and increases the energy density.

Recovering and/or recycling water from the cathode reaction has been used to dilute pure methanol in direct methanol fuel cells [32–34], but onboard hydrogen generation by recycling byproduct water has not been studied. In this work, a new method for generating hydrogen onboard by recycling water from the cathode reaction was studied. As depicted in Fig. 1, the micro-power generator comprises a hydride fuel chamber and a PEM fuel cell. Due to the hygroscopic nature of hydride on the anode of the fuel cell and the byproduct water on the cathode, a concentration gradient of water vapor is established across the proton exchange membrane (Nafion®). The water recovery is carried out by water diffusion from the more humid cathode side to the less humid anode side. The hydride in the fuel chamber utilizes the byproduct water generated on the cathode to generate hydrogen without an external water supply. The purpose of this paper is to describe this onboard hydrogen generation method by recycling water from the cathode reaction for developing high energy density micro-power generators with onboard fuels.

In this work, the proton exchange membrane fuel cells were made of commercial Nafion 111 (25 μm thick) and 112 (50 μm thick), and 25 μm thick stainless steel sheets were used as support structures and current collectors. CaH_2 and $LiAlH_4$ were chosen as model hydrides to perform the experimental work. First, the water recovery micro-fuel cell (WRMFC) was tested at different relative humidity at room temperature. The performance of the WRMFC – polarization curve, current density at 0.5 V, and the proton conductivity – was measured by a potentiostat. Then WRMFCs with different opening areas, different hydrides, and different Nafion membranes were tested at three different relative humidities. Finally, 10 mm^3 WRMFCs were built and life time tests were performed.

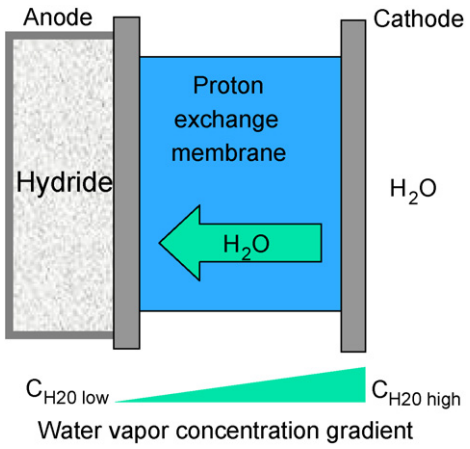

Fig. 1. Schematic of the hydrogen generation and water transport mechanism in a water recovery micro-PEM fuel cell. The water vapor concentration gradient was created by the byproduct water on the cathode and the hygroscopic hydride on the anode. The hydride in the fuel chamber utilizes the byproduct water generated on the cathode of the fuel cell to generate hydrogen without an external water supply.

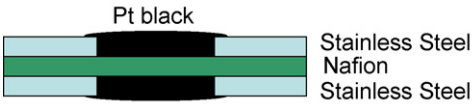

Fig. 2. Schematic of the membrane electrode assembly (MEA) used in this work. The MEA is comprised of a Nafion® proton exchange membrane, platinum black in a nafion-based ink as the catalyst, and two stainless steel sheets as the support structures and current collectors. The Nafion membrane was sandwiched between two thin stainless steel sheets by adhesive bonding.

2. Experimental

2.1. Membrane electrode assembly

As shown in Fig. 2, the membrane electrode assembly (MEA) for the hydrogen PEM fuel cell is comprised of a Nafion proton exchange membrane, platinum black in a Nafion-based ink as the catalyst, and two stainless steel sheets as support structures and current collectors. The Nafion membrane was sandwiched between two thin stainless steel plates by adhesive bonding [35]. Catalyst inks were prepared by dispersing platinum black (HiSPEC 1000, Alfa Aesar, Ward Hill, MA) with Nafion solution, Millipore water, and isopropanol via sonication. Using the direct painting method, the catalyst inks were painted onto the Nafion layer of the anode and cathode to form the membrane electrode assembly. The resulting catalyst loading was approximately 20 $mg\,cm^{-2}$. In addition to the membrane area, a small amount of catalyst ink was painted onto the stainless steel current collectors to provide electrical connection.

2.2. Humidity controlled box

A humidity controlled box was made to test the device performance at different relative humidities, as shown in the schematic in Fig. 3. Both dry and humidified air are supplied from compressed dry air cylinders and a water bubbler was used to humidify air in one line. The relative humidity in the box was controlled by adjusting the flow rates of dry air and humidified air, which are delivered to the box through a Tee-connector. An SHT75 digital humidity and

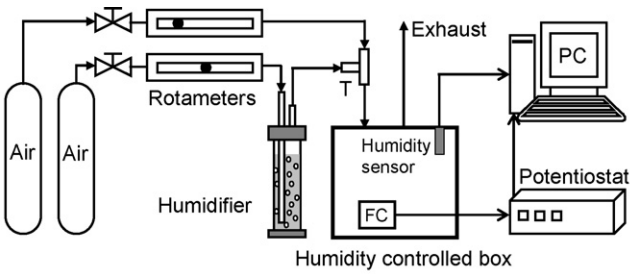

Fig. 3. Schematic of a humidity controlled box. The relative humidity in the box was controlled by adjusting the flow rates of dry air and humidified air, which are delivered to the box through a T connector. The humidity inside the box is monitored and recorded by an SHT75 digital humidity and temperature sensor.

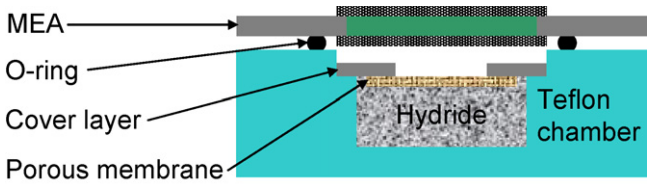

Fig. 4. Schematic of a testing package with an onboard hydride and a MEA. The Teflon chamber was used to contain hydride fuels, the cover layer (50 μm stainless steel sheet) with porous hydrophobic PTFE membrane was used to prevent hydride powder from touching MEA directly, and the system was sealed by O-rings.

temperature sensor (Sensirion Inc., Switzerland) was used to monitor and record the relative humidity and temperature inside the box.

2.3. Fuel cell testing

The schematic of a testing package with an onboard hydride and a MEA is shown in Fig. 4. This package was reused to construct the prototype WRMFCs and perform the characterization. The Teflon chamber was used to contain hydride fuels, the cover layer (50 μm stainless steel sheet) with porous hydrophobic PTFE membrane (GE Osmonics Labstore, Minnetonka, MN) was used to prevent hydride powder from touching the MEA directly, and the system was sealed by O-rings. Both CaH_2 and $LiAlH_4$ were purchased from Aldrich Chemical Company (St. Louis, MO). The hydrides were loaded into the Teflon chamber inside a dry nitrogen glove box (Labconco, Kansas City, Missouri), since the hydrides can react with the moist air to generate hydrogen. The prototype WRMFC was tested using a Solartron SI 1287 potentiostat (Solartron Analytical, Hampshire, UK). All the tests were performed near room temperature (~22 °C).

3. Experimental results

Fig. 5 shows the polarization curves and power density plots of two MEAs with Nafion 111 and 112. The hydrogen was supplied from a compressed hydrogen cylinder and the oxygen was from the ambient air. The MEA with Nafion 111 has an open cell potential (the voltage output of the fuel cell in the zero current density limit) of 0.98 V and a peak power density of 118 mW cm^{-2}. The MEA with Nafion 112 has an open cell potential of 1 V and a peak power density of 109 mW cm^{-2}. In this study, the MEA with Nafion 111 and CaH_2 were chosen to perform subsequent tests with different relative humidity and opening areas. The performances of the WRMFC with different Nafion membranes and different hydrides were also compared. Fig. 6 shows a typical polarization curve of a WRMFC

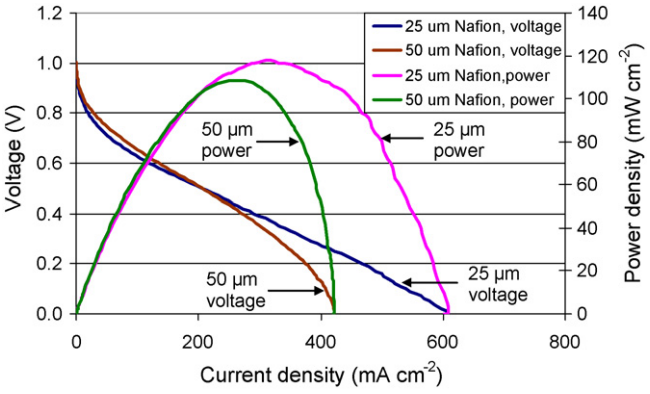

Fig. 5. Polarization curves and power density plots of two MEAs with Nafion 111 (25 μm) and 112 (50 μm). Hydrogen is supplied from a hydrogen tank, and oxygen is from the ambient air.

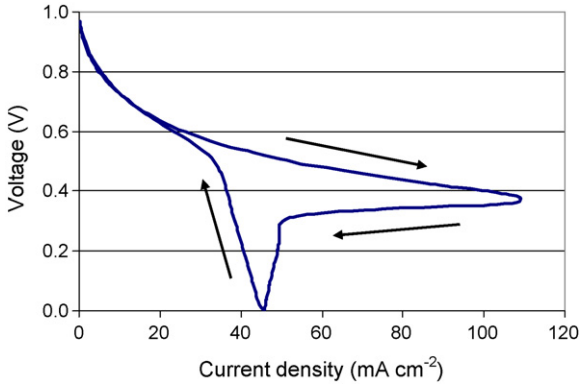

Fig. 6. A typical polarization curve of a WRMFC with Nafion 111 membrane, CaH_2 fuel, and 4 mm diameter opening area at 45% relative humidity. A potentiostat was used to control the output voltage of the fuel cell and to measure the resulting output current density at each scanning voltage. The potentiostat sweeps from open cell potential to short circuit, then sweeps back from short circuit to open cell potential at a scanning rate of 10 mV s^{-1}.

with Nafion 111 membrane, CaH_2 fuel, and 4 mm diameter opening area at 45% relative humidity. In this experiment, a potentiostat was used to control the output voltage of the fuel cell, and measure the resulting output current density. The potentiostat sweeps from open cell potential to short circuit, then sweeps back from short circuit to open cell potential with a scanning rate of 10 mV s^{-1}. Current density is measured and recorded at each scanning point.

A WRMFC with Nafion 111 membrane, CaH_2 fuel, and 4 mm diameter opening area was tested in the humidity controlled box at different relative humidities. The polarization curve and current density at 0.5 V of the WRMFC was measured by a Solartron SI 1287 potentiostat. The proton conductivity of the WRMFC was measured with an AC impedance measurement [36]. Fig. 7 shows the polarization curves (the potentiostat sweeps from 0.1 V to open cell potential) of this WRMFC at nine different humidity levels from 5% to 90%. The polarization curve at 5% relative humidity does not appear to have reached a hydrogen mass transport limit, but the others demonstrate clear mass transport limit. The maximum current density due to the mass transport limit increased as the relative humidity is increased. From these polarization curves, we also can see different performances of the WRMFC at different relative humidity levels. Fig. 8 shows the change in proton conductivity and the current density at 0.5 V of this WRMFC with increasing relative humidity.

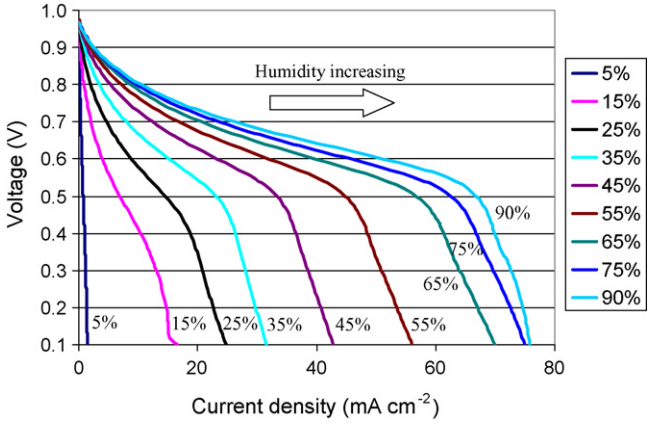

Fig. 7. The polarization curves (from 0.1 V to open cell potential) of a WRMFC at nine different humidity levels from 5% to 90%. The polarization curve at 5% relative humidity does not have a hydrogen mass transport limit, but the others have clear mass transport limit. The maximum current density due to the mass transport limit increases as the relative humidity is increased.

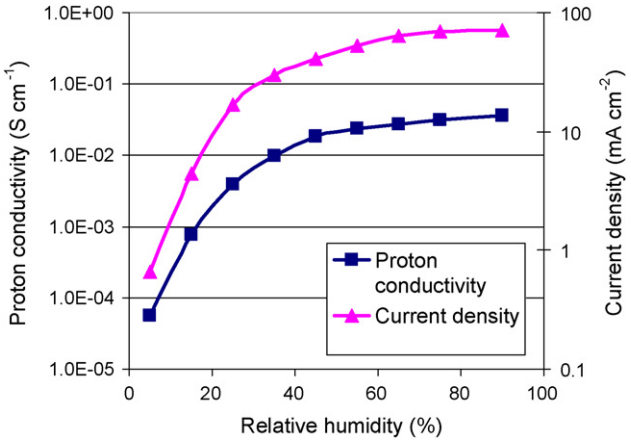

Fig. 8. Proton conductivity and the current density at 0.5 V of a WRMFC at nine different humidity levels from 5% to 90%. The proton conductivity and the current density at 0.5 V of this WRMFC increases as the relative humidity is increased. The proton conductivity of the WRMFC decreases drastically as the relative humidity is lower than 25%.

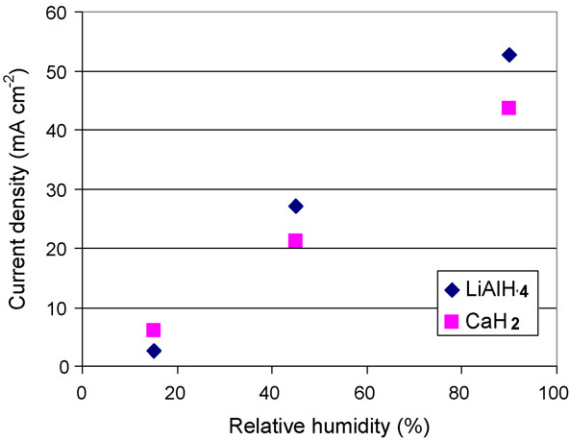

Fig. 10. A comparison of current density at 0.5 V of a WRMFC with CaH_2 and $LiAlH_4$ fuels. The devices with a 2 mm diameter opening area were tested at three different humidities. At 15% relative humidity, the current density with CaH_2 is higher than that with $LiAlH_4$, while the current density with $LiAlH_4$ is higher than that with CaH_2 at 45% and 90% relative humidity.

In order to control the hydrogen generation rate, control mechanisms have to be studied. As shown in Fig. 4, after the MEA has been made and mounted to the package, the only parameter that can be changed is the opening area on the cover layer. In this work, three devices with three different opening areas, 1 mm diameter, 2 mm diameter, and 4 mm diameter, were tested at different relative humidities. Fig. 9 shows the current densities at 0.5 V of the WRMFCs with three different opening areas at three different humidity levels. At 15% relative humidity, the device with 4 mm diameter opening has current density between the other two devices. At 45% and 90% relative humidity, the current density at 0.5 V is higher for the larger opening areas.

As demonstrated in our previous work [17], $LiAlH_4$ also has a more complete hydrolysis reaction with pure water. In this work, a WRMFC with Nafion 111 membrane and 2 mm diameter opening area was loaded with $LiAlH_4$ powder and tested. The comparison of current density at 0.5 V with CaH_2 and $LiAlH_4$ fuels is shown in Fig. 10. At 15% relative humidity, the current density with CaH_2 is higher than that with $LiAlH_4$, while the current density with $LiAlH_4$ is higher than that with CaH_2 at 45% and 90% relative humidity. The WRMFC with Nafion 112 membrane, CaH_2 fuels, and 2 mm diameter opening area was also tested. As shown in Fig. 11, the device with

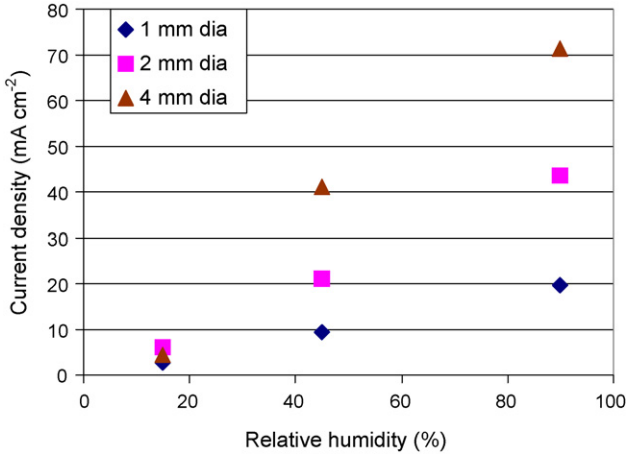

Fig. 9. The current densities at 0.5 V of a WRMFC with three different opening areas at three different humidities. At 15% relative humidity, the device with 4 mm diameter opening has current density in between the other devices. At 45% and 90% relative humidity, the current density at 0.5 V is higher with bigger opening areas.

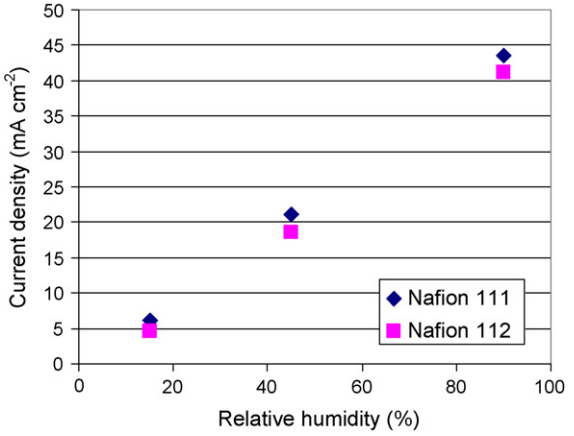

Fig. 11. A comparison of current density at 0.5 V of a WRMFC with Nafion 111 and Nafion 112 membranes. The device has a 2 mm diameter opening area and was tested with CaH_2 fuels at three different humidities. The device with Nafion 112 shows slightly lower current density at 0.5 V than the device with Nafion 111.

Nafion 112 shows slightly lower current density at 0.5 V than the device with Nafion 111.

As mentioned above, this water recovery method paves the way for achieving higher energy densities for micro-fuel cells. The schematic of a 10 mm^3 integrated device is shown in Fig. 12. It consists of a hydrogen generator connected to a fuel cell. CaH_2

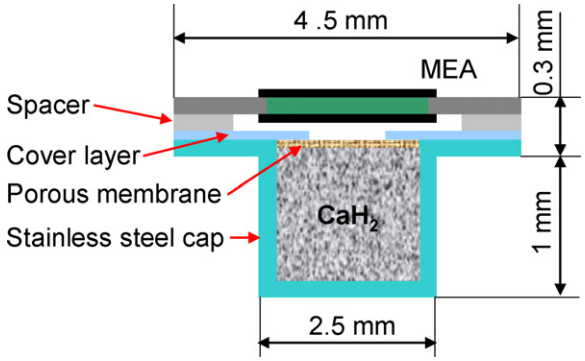

Fig. 12. Schematic of a 10 mm^3 WRMFC. CaH_2 is loaded into the stainless steel cap in a dry nitrogen glove box.

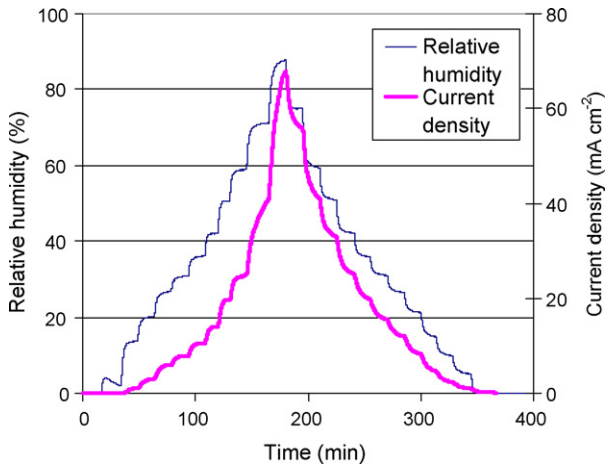

Fig. 13. The current density of a 10 mm^3 integrated devices with 0.2 mm^2 opening areas on the cover layer at different relative humidity. The current density of this WRMFC is very sensitive to the relative humidity.

was loaded into the stainless steel cap in a dry nitrogen glove box (Labconco, Kansas City, Missouri). Fig. 13 shows the current density of a 10 mm^3 devices with 0.2 mm^2 opening area on the cover layer at different relative humidities. The current density of this WRMFC is very sensitive to the relative humidity. As can be seen from Fig. 13, the current density changes immediately when the relative humidity changes. Fig. 14 shows the life time test results of two 10 mm^3 devices with 0.2 mm^2 and 0.4 mm^2 opening areas on the cover layer, respectively. The tests were performed at constant 50% relative humidity. Since both of the devices were operated in the mass transport limit region, the current density is the highest at the beginning and gradually decreased to zero in several hours. The maximum power density is 104 W L^{-1}, and the maximum energy density is 313 W h L^{-1}. The burst of current at the beginning is because the hydrogen was generated and pressurized inside the stainless steel cap during transferring the devices from dry glove box to the humidity controlled box. After the accumulated hydrogen was consumed by the fuel cell at relatively high current, the current dropped to the hydrogen generation limit region.

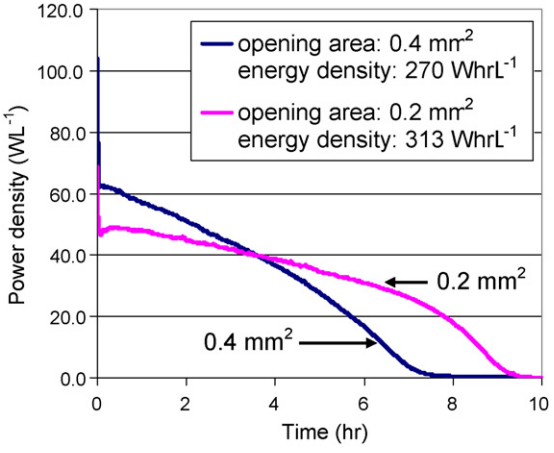

Fig. 14. Life time test results of two 10 mm^3 integrated devices with 0.4 mm^2 and 0.2 mm^2 opening areas on the cover layer, respectively. The tests were performed at constant 50% relative humidity. Since both of the devices were operated in the mass transport limit region, the current density is highest at the beginning and gradually decreased to zero in several hours. The maximum power density is 104 W L^{-1}, and the maximum energy density is 313 W h L^{-1}.

4. Discussion

The results show further evidence that WRMFCs can meet both the energy and power density requirements for micro-power applications. As shown in Table 1, the theoretical volumetric energy density of some hydride fuels without onboard water can be above 2000 W h L^{-1}, which is four times higher than the current lithium ion batteries [37]. However, the performance of the MEA with pure hydrogen is better than the WRMFC with hydride on the anode, as shown in Figs. 5 and 7. This lower performance results from the presence of a hygroscopic hydride on the anode dehydrating the MEA and thereby decreasing the proton conductivity, especially at low humidity. In addition, the water diffusion rate through the MEA also limits the performance. These problems can be addressed by utilizing self-hydration and thinner MEAs [38] in future designs. A typical polarization curve of a WRMFC at 45% relative humidity is shown in Fig. 6. The current starts from a low current level of microampere and increases as the potentiostat sweeps from an open cell potential to short circuit. The low current can cause hydrogen accumulation at the beginning because the WRMFC also can get water from atmosphere to generate hydrogen. The accumulated hydrogen extends the current region beyond the level of hydrogen transport limit in the polarization curve. After the accumulated hydrogen is consumed, the current drops to the level of hydrogen transport limit. When the potentiostat sweeps from short circuit to open cell potential, there is no hydrogen accumulation at the beginning and the current starts from the level of hydrogen transport limit. As shown in Fig. 7, the performance of the WRMFC is strongly affected by the relative humidity, because the byproduct water that is recovered and converted to hydrogen via the hydrolysis reaction is related to the relative humidity. The byproduct water can evaporate into the ambient air, while the water vapor in the ambient air also can diffuse into the hydride chamber through the Nafion membrane. Only after equilibrium is reached, can all of the byproduct water be recovered, and no additional water from the ambient diffuses into the hydride chamber. However, the relative humidity strongly affects the equilibrium state and the water diffusion rate through the Nafion as a function of the relative humidity.

As shown in Fig. 8, the proton conductivity of the WRMFC decreases drastically when the relative humidity is lower than 25%. Compared to the proton conductivity of Nafion 117 (175 μm thick) at different relative humidities shown in literature [39], the MEA in the water recovery device has lower proton conductivity. The lower conductivity is due to the desiccating nature of the hygroscopic hydride directly on the anode of the MEA, which decreases the proton conductivity by dehydrating the MEA. The current density at 0.5 V shows a similar trend as the proton conductivity at low humidity levels, because it is mainly determined by the low proton conductivity. At 5% relative humidity, the polarization curve does not have a mass transport limit, because the hydrogen generation rate is higher than the maximum hydrogen consumption rate by the fuel cell. As the relative humidity was higher than 15%, the hydrogen generation rate is linearly related to the relatively humidity and produces a current density with a linear trend. However, the current density curve starts to flatten out as the relative humidity is higher than 65%. This behavior may be due to strong electroosmotic drag at high current levels [40,41], which can pull water with protons from the anode to the cathode. This opposite water transport slows down water diffusion from the cathode to the anode.

Fig. 9 shows the performance of a water recovery device with three different opening areas: 1, 2, and 4 mm in diameter. The device with the largest opening has a higher performance at high relative humidity, but a lower performance at low humidity. The larger exposed area to the hydride causes lower proton conductivity at low relative humidity, which dominates the fuel cell performance. However, the current density is not proportional to the opening area,

which shows that the opening area is not the only factor affecting water diffusion through the Nafion membrane. Other factors, such as the area of the Nafion membrane, electroosmotic drag at high current, and the distance between the Nafion and the hydride, also play important roles.

Fig. 10 shows that the device with $LiAlH_4$ has a higher performance at high relative humidities, but a lower performance at lower humidities, compared to the device with CaH_2. This phenomenon can be explained by the powder size of these two hydrides. $LiAlH_4$ has a much smaller powder size than CaH_2, resulting in a larger exposed area to water vapor. At low relative humidity, the larger exposed surface area of the $LiAlH_4$ powder causes lower proton conductivity and dominates the performance of the fuel cell. At high relative humidities, the larger exposed surface area of the $LiAlH_4$ powder results in a higher hydrogen generation rate and increases the performance of the fuel cell. Fig. 11 shows that the device with Nafion 111 has a slightly higher performance than the device with Nafion 112. The hydrogen generation rate, corresponding to the water diffusion rate through the MEA, increases with a thinner MEA. However, the thickness of the catalyst layers also can affect water diffusion. Since the catalyst layers are about 50 μm thick and the Nafion membrane is 25–50 μm thick, the catalyst layers could be the dominant factors.

As shown in Figs. 13 and 14, the maximum energy density is 313 W h L^{-1} for a WRMFC with a 38% volumetric ratio of fuel chamber to device. This energy density is higher than the energy density of our previous devices with onboard water [29,31], but it is still much lower than the theoretical energy density of 740 W h L^{-1} if the fuel chamber were completely filled with CaH_2 fuels. In this work, the fuel chamber was not completely filled with hydride because volume expansion of the hydride reactant to hydrate product can break the epoxy bonding holding the chamber to the MEA. In addition, some hydrogen may be lost due to the hydrogen crossover through the MEA.

5. Conclusion

An onboard hydrogen generation method by recycling water from the cathode reaction was introduced in this paper. Water-recovery micro-fuel cells were constructed and tested. The results show that this method can be used to build high energy density power sources for micro-scale applications in the future. Although the performance of the WRMFCs is affected strongly by the relative humidity, about 1 mW power has been generated by an MEA with 12.6 mm^2 area at 25% relative humidity. The performance of water recovery devices is mainly determined by the proton conductivity of the MEA at low humidity and by the water diffusion rate through the MEA at high humidity. In addition, an opposing electroosmotic drag also can affect the water diffusion rate from the cathode to the anode if the current density is high. The opening area on the cover layer can also affect the performance of the water recovery devices, and this phenomenon can be used to control the hydrogen generation rate by integrating feedback control mechanisms into these devices to control the opening area. Two hydrides, CaH_2 and $LiAlH_4$, have been studied in the WRMFCs. A 10 mm^3 prototype WRMFC has been built and tested. A maximum power density of 104 W L^{-1} and a maximum energy density of 313 W h L^{-1} have been produced by the WRMFCs.

Acknowledgements

This work was supported by the Defense Advanced Research Projects Agency, under contract DST 2007-0299513-000. Any opinions, findings, and conclusions or recommendations expressed in this manuscript are those of the authors and do not necessarily reflect the views of the Defense Advanced Projects Research Agency.

References

[1] K. Cowey, K.J. Green, G.O. Mepsted, R. Reeve, Curr. Opin. Solid St. M. 8 (2004) 367–371.
[2] G. Erdler, M. Frank, M. Lehmann, H. Reinecke, C. Muller, Sens. Actuators A 132 (2006) 331–336.
[3] S.F.J. Flipsen, J. Power Sources 162 (2006) 927–934.
[4] A. Heinzel, C. Hebling, M. Muller, M. Zedda, C. Muller, J. Power Sources 105 (2002) 250–255.
[5] J.D. Morse, Int. J. Energy Res. 31 (2007) 576–602.
[6] J.S. Wainright, R.F. Savinell, C.C. Liu, M. Litt, Electrochim. Acta 48 (2003) 2869–2877.
[7] C. Wang, Z.Q. Mao, R.H. Chen, G.H. Wang, X.F. Xie, Prog. Chem. 18 (2006) 30–35.
[8] U.S. Department of Energy, Fuel Cells, and Infrastructure Technologies, Multi-Year Research, Development and Demonstration Plan: Planned Program Activities for 2004–2015, 2003.
[9] F.L. Darkrim, P. Malbrunot, G.P. Tartaglia, Int. J. Hydrogen Energy 27 (2002) 193–202.
[10] C. Liu, Y.Y. Fan, M. Liu, H.T. Cong, H.M. Cheng, M.S. Dresselhaus, Science 286 (1999) 1127–1129.
[11] A.C. Dillon, K.M. Jones, T.A. Bekkedahl, C.H. Kiang, D.S. Bethune, M.J. Heben, Nature 386 (1997) 377–379.
[12] N.L. Rosi, J. Eckert, M. Eddaoudi, D.T. Vodak, J. Kim, M. O'Keeffe, O.M. Yaghi, Science 300 (2003) 1127–1129.
[13] M. Ni, D.Y.C. Leung, M.K.H. Leung, Int. J. Hydrogen Energy 32 (2007) 3238–3247.
[14] M.J. Varady, L. McLeod, J.M. Meacham, F.L. Degertekin, A.G. Fedorov, J. Micromech. Microeng. 17 (2007) S257–S264.
[15] P. Muthukumar, M.P. Maiya, S.S. Murthy, Int. J. Hydrogen Energy 30 (2005) 1569–1581.
[16] B. Sakintuna, F. Lamari-Darkrim, M. Hirscher, Int. J. Hydrogen Energy 32 (2007) 1121–1140.
[17] L. Zhu, D. Kim, H. Kim, R.I. Masel, M.A. Shannon, J. Power Sources 185 (2008) 1334–1339.
[18] S.D. Richardson, T.A. Ternes, Anal. Chem. 77 (2005) 3807–3838.
[19] D. Gervasio, S. Tasic, F. Zenhausern, J. Power Sources 149 (2005) 15–21.
[20] J.C. McDonald, D.C. Duffy, J.R. Anderson, D.T. Chiu, H.K. Wu, O.J.A. Schueller, G.M. Whitesides, Electrophoresis 21 (2000) 27–40.
[21] A. Pinto, D.S. Falcao, R.A. Silva, C.M. Rangel, Int. J. Hydrogen Energy 31 (2006) 1341–1347.
[22] J.L. Zhang, Y.H. Tang, C.J. Song, Z.T. Xia, H. Li, H.J. Wang, J.J. Zhang, Electrochim. Acta 53 (2008) 5315–5321.
[23] Y. Kojima, K. Suzuki, K. Fukumoto, Y. Kawai, M. Kimbara, H. Nakanishi, S. Matsumoto, J. Power Sources 125 (2004) 22–26.
[24] A.V. Pattekar, M.V. Kothare, J. Microelectromech. Syst. 13 (2004) 7–18.
[25] X.Z. Yuan, H.J. Wang, J.C. Sun, J.J. Zhang, Int. J. Hydrogen Energy 32 (2007) 4365–4380.
[26] S.C. Amendola, S.L. Sharp-Goldman, M.S. Janjua, N.C. Spencer, M.T. Kelly, P.J. Petillo, M. Binder, Int. J. Hydrogen Energy 25 (2000) 969–975.
[27] S.C. Amendola, S.L. Sharp-Goldman, M.S. Janjua, M.T. Kelly, P.J. Petillo, M. Binder, J. Power Sources 85 (2000) 186–189.
[28] V.C.Y. Kong, D.W. Kirk, F.R. Foulkes, J.T. Hinatsu, Int. J. Hydrogen Energy 28 (2003) 205–214.
[29] S. Moghaddam, E. Pengwang, K.Y. Lin, R.I. Masel, M.A. Shannon, J. Microelectromech. Syst. 17 (2008) 1388–1395.
[30] V. Swaminathan, L. Zhu, B. Gurau, R.I. Masel, M.A. Shannon, IEEE MEMS, Sorento, Italy, 2009, pp. 35–38.
[31] L. Zhu, K.Y. Lin, R.D. Morgan, V.V. Swaminathan, H.S. Kim, B. Gurau, D. Kim, B. Bae, R.I. Masel, M.A. Shannon, J. Power Sources 185 (2008) 1305–1310.
[32] S.C. Yao, X.D. Tang, C.C. Hsieh, Y. Alyousef, M. Vladimer, G.K. Fedder, C.H. Amon, Energy 31 (2006) 636–649.
[33] R.Z. Jiang, D. Chu, J. Electrochem. Soc. 155 (2008) 804–810.
[34] H. Kim, J. Oh, J. Kim, H. Chang, J. Power Sources 162 (2006) 497–501.
[35] B.R. Flachsbart, K. Wong, J.M. Iannacone, E.N. Abante, R.L. Vlach, P.A. Rauchfuss, P.W. Bohn, J.V. Sweedler, M.A. Shannon, Lab Chip 6 (2006) 667–674.
[36] T.E. Springer, T.A. Zawodzinski, M.S. Wilson, S. Gottesfeld, J. Electrochem. Soc. 143 (1996) 587–599.
[37] R. Hahn, in: A.E. Léon (Ed.), Hydrogen Technology: Mobile and Portable Applications, Springer, Berlin, 2008, pp. 380–408.
[38] X.B. Zhu, H.M. Zhang, Y. Zhang, Y.M. Liang, X.L. Wang, B.L. Yi, J. Phys. Chem. B 110 (2006) 14240–14248.
[39] Y. Sone, P. Ekdunge, D. Simonsson, J. Electrochem. Soc. 143 (1996) 1254–1259.
[40] Z.W. Dunbar, R.I. Masel, J. Power Sources 171 (2007) 678–687.
[41] Z.W. Dunbar, R.I. Masel, J. Power Sources 182 (2008) 76–82.